Retinal Pigment Epithelium Defects Accelerate Photoreceptor Degeneration in Cell Type–Specific Knockout Mouse Models of Choroideremia

Tanya Tolmachova,[1] *Silene T. Wavre-Shapton,*[1,2] *Alun R. Barnard,*[3] *Robert E. MacLaren,*[3,4] *Clare E. Futter,*[2] *and Miguel C. Seabra*[1,5,6]

Purpose. Choroideremia (CHM) is a progressive X-linked degeneration of three ocular layers (photoreceptors, retinal pigment epithelium, and choroid), with a complex and still largely unclear pathogenesis. To investigate the pathophysiology of CHM, the authors engineered mice with a cell type–specific *Chm/Rep1* knockout (KO).

Methods. A mouse line carrying a conditional allele Chm^{Flox} was crossed with the transgenic line *IRBP-Cre* to achieve *Chm* KO, specifically in the photoreceptor layer, and *Tyr-Cre* to produce *Chm* KO, specifically in the retinal pigment epithelial and other pigmented cells. Chm^{Flox}, *Tyr-Cre*+ and Chm^{Flox}, *IRBP-Cre*+ mice were mated to produce mice with *Chm* KO in both layers. All mouse lines were studied by histology, electron microscopy, electroretinography (ERG), scanning laser ophthalmoscopy (SLO), and biochemical methods.

Results. In Chm^{Flox}, *IRBP-Cre*+ mice the authors observed the progressive degeneration of photoreceptors in the presence of normal retinal pigment epithelium (RPE). Chm^{Flox}, *Tyr-Cre*+ mice exhibited coat color dilution and pigment abnormalities of the RPE in the presence of an intact outer nuclear layer. In 6- to 8-month-old Chm^{Flox}, *Tyr-Cre*+, *IRBP-Cre*+ mice, the degeneration of photoreceptors was accelerated compared with Chm^{Flox}, *IRBP-Cre*+ mice but became leveled with age, such that it was comparable at 12 to 14 months. Detailed ERG and SLO analysis supported the histopathologic findings.

Conclusions. Defects in photoreceptors and RPE can arise because of intrinsic defects caused cell autonomously by the *Chm* KO. However, when both photoreceptors and RPE are diseased, the dynamics of the degenerative process are altered. Photoreceptor functional deficit and cell death manifest much earlier, suggesting that the diseased RPE accelerates photoreceptor degeneration. (*Invest Ophthalmol Vis Sci.* 2010;51: 4913–4920) DOI:10.1167/iovs.09-4892

Choroideremia (CHM) is an X-linked progressive retinal degeneration affecting approximately 1 in 50,000 persons.[1–4] The first symptoms include night blindness in teenage patients, followed by constriction of the visual field and progressive loss of vision within the next two to three decades. With no cure currently available, most patients are legally blind by their mid-40s. When examined, carrier females exhibit characteristic changes of the fundus but are predominantly asymptomatic, with rare severe cases that are presumably caused by skewed X-inactivation.[5–7]

The *CHM/REP1* gene is the causative gene in CHM patients and is positioned at the locus Xq21.2.[8] The *Chm* gene product, also known as Rab Escort Protein 1 (REP1), assists in the lipid modification of Rab GTPases. This modification, known as prenylation, involves the covalent attachment of one or two prenyl groups (geranylgeranyl or farnesyl) to the C terminus of a Rab protein.[9] Catalytic function is performed by the enzyme Rab geranylgeranyl transferase (Rab GGTase) and REP1 assists in the reaction by binding unprenylated Rab substrates to Rab GGTase and then delivering newly prenylated Rab to a specific membrane.[10]

Rabs are small GDP/GTP-binding proteins that are inactive when bound to GDP and that change their conformation when GDP is displaced by GTP.[11] Activation through GTP-binding leads to the recruitment of effectors, which results in downstream biological effects.[12] In humans, the Rab family includes more than 60 known members,[13] whereas other species such as mouse, rat, zebrafish, and yeast also have extensive Rab families. Their main role is to regulate intracellular vesicular transport; prenylation is a prerequisite for their functionality because it provides the hydrophobicity that allows Rabs to bind membranes.[14,15]

CHM/REP1 loss-of-function mutations in humans lead solely to eye disease. No other tissue or organ has been reported to be affected, presumably because of the functional redundancy provided by the presence of another protein, REP2, also known as CHML (choroideremia-like protein). Both REP1 and REP2 are ubiquitously expressed and have 75% amino acid identity and 90% similarity.[16] *Chm* knockout (KO) appears to be more severe in animal models. In mice, the *Chm* KO is embryonically lethal because of abnormalities in extraembryonic mouse tissues such as placenta and yolk sac despite the presence of the *Chml* gene.[17] Nevertheless carrier females ($Chm^{null/WT}$) are viable and exhibit progressive retinal degeneration.[18,19] In zebrafish, *Chml/Rep2* is not present, and *Chm* KO manifests as an extremely severe systemic illness leading to early lethality at postnatal day 6, which limits its use as a model of CHM.[20,21]

With three affected eye layers that are interdependent (choroid, photoreceptors, and RPE), the pathogenesis of CHM is complex and remains unclear. One possibility is that CHM originates in one layer (primary site of degeneration),

From the [1]Molecular Medicine Section, National Heart and Lung Institute, Imperial College London, London, United Kingdom; [2]UCL Institute of Ophthalmology, London, United Kingdom; [3]Nuffield Laboratory of Ophthalmology, University of Oxford, Oxford, United Kingdom; [4]Moorfields Eye Hospital—UCL Institute of Ophthalmology NIHR Biomedical Research Centre, London, United Kingdom; [5]CEDOC, Faculdade de Ciências Médicas, Universidade Nova de Lisboa, Lisboa, Portugal; and [6]Instituto Gulbenkian de Ciência, Oeiras, Portugal.

Supported by the Wellcome Trust, Choroideremia Research Foundation, and Fight for Sight (Tommy Salisbury Fund). MCS is the recipient of a Gulbenkian Mid-Career Fellowship.

Submitted for publication November 10, 2009; revised February 25, 2010; accepted March 30, 2010.

Disclosure: **T. Tolmachova**, None; **S.T. Wavre-Shapton**, None; **A.R. Barnard**, None; **R.E. MacLaren**, None; **C.E. Futter**, None; **M.C. Seabra**, None

Corresponding author: Miguel C. Seabra, Molecular Medicine Section, National Heart and Lung Institute, Imperial College London, London SW7 2AZ, United Kingdom; m.seabra@imperial.ac.uk.

which then leads to the demise of the other two layers. The RPE is the most likely candidate for the primary site of degeneration given its position between the other two degenerating layers.[22] Another hypothesis is that the disease appears in the RPE and photoreceptors simultaneously (cell autonomously).[19,23] In our previous study,[19] we generated mouse CHM carriers (*Chm*$^{null/WT}$) and two conditional alleles (*Chm*^{Flox} and *Chm*^{3lox}) that were crossed with *six3-Cre* and inducible *MerCreMer* transgenic lines. We showed that in the RPE and the neuroretina, different subsets of Rabs are underprenylated, implying that both layers have intrinsic prenylation defects.[19] To investigate the pathogenesis of the disease further, we generated two new mouse models in which *Chm* KO is achieved specifically in the RPE (and other pigmented cells) or photoreceptors. The aim of our study was to investigate whether the *Chm* KO in one layer (either the photoreceptors or the RPE) could initiate or affect the degeneration of the other layer.

Methods

Mice

All mice used in this study were treated humanely and in accordance with the UK Home Office Regulations under project license 70/6176. Care, use, and treatment of the animals were in strict agreement with the ARVO Statement for the Use of Animals in Ophthalmic and Vision Research. Mice with *Chm*^{Flox} and *Chm*^{3lox} alleles and tamoxifen (TM)-inducible *MerCreMer* transgene have been described previously.[19] The transgenic *IRBP-Cre* mouse line expresses a *Cre*-transgene under the control of the human *IRBP* promoter.[24] The transgenic *Tyr-Cre* mouse line (Tyr::CreB), with the *Cre*-recombinase gene under the control of a tyrosinase promoter, was described previously.[25] The tyrosinase promoter is a fusion between 2.5 kb of the region immediately upstream of the first exon of the tyrosinase gene and the 3.6-kb enhancer located 15 kb upstream of the first exon. Routine genotyping of mice by PCR was described previously.[19] Primers H7 (5′-agagtatctcagcagtagctctcc) and H9 (5′-ccagagaacactgagggttagagc) allowed the identification of *Chm*^{WT}, *Chm*^{Flox}, and *Chm*^{null} alleles. Sizes of the resultant PCR products were 780 bp (*Chm*^{WT}), 860 bp (*Chm*^{Flox}), and 330 bp (*Chm*^{null}). To identify the *Tyr-Cre* transgene, we used primers LL125 (5′-gtcactccaggggttgctgg) and Cre3 (5′-caacttgcaccatgccgccc); the size of the product was 150 bp. For the *IRBP-Cre* transgene, we used Cre3 and IRBP4 (5′-gatacccagggttgatgtgc); the size of the product was 230 bp. *Cre*-specific primers Cre1 (5′-tcccgcagaacctgaagatgttc) and Cre2 (5′-ggatcatcagctacaccagagacg) were used to screen for the *MerCreMer* transgene (510-bp product).

In Vitro Prenylation Assay and Immunoblot

The in vitro prenylation assay was performed on cytosolic fractions of tissue and cell lysates that were collected after ultracentrifugation (100,000*g*, 1 hour, 4°C). The assay was performed in a 25-μL reaction

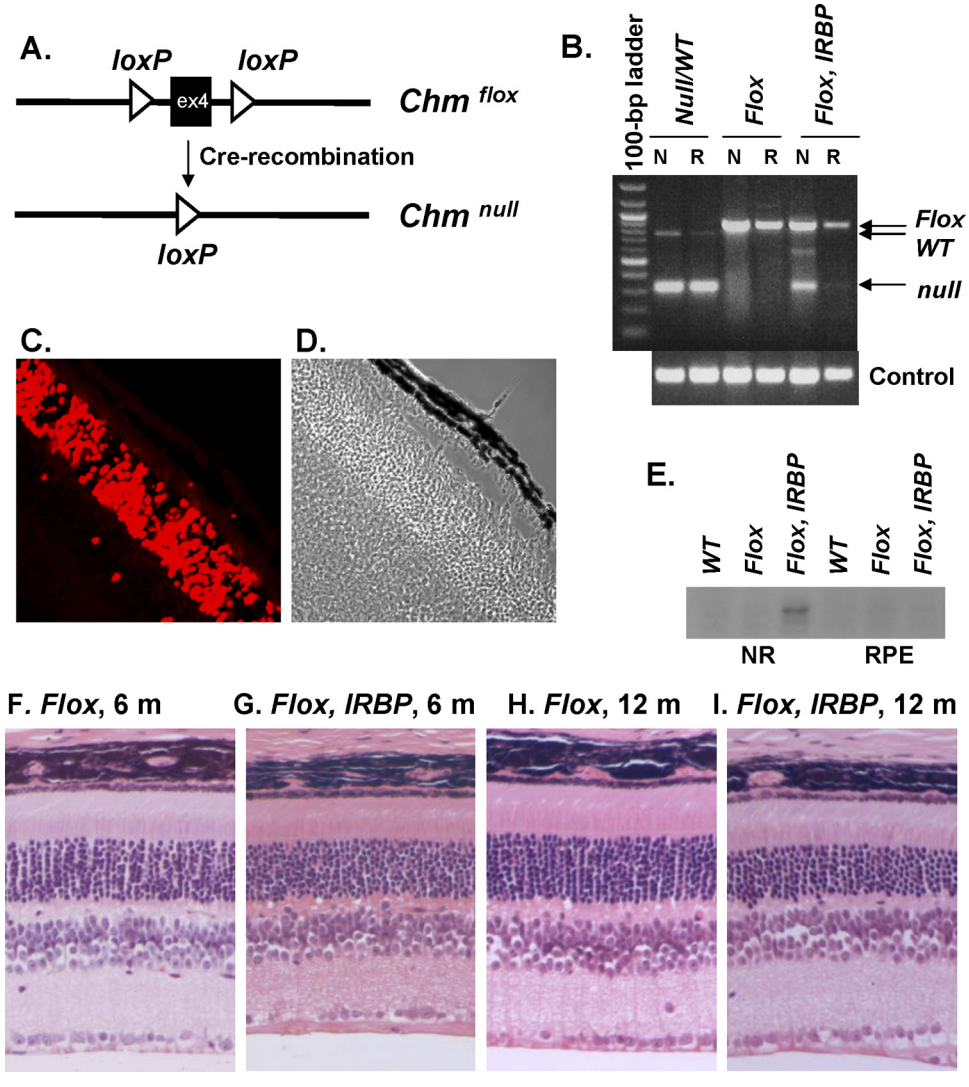

Figure 1. Characterization of *Chm*^{Flox}, *IRBP-Cre*+ model. (**A**) Illustration showing main features of the *Chm*^{Flox} allele and its conversion to the *Chm*^{Null} allele after *Cre*-recombination. (**B**) Neuroretina (N) and RPE (R) were isolated from the eyes of *Chm*$^{Null/WT}$, *Chm*^{Flox}, *Chm*^{Flox}, *IRBP-Cre*+ animals and analyzed by PCR using primers that could identify *Chm*^{Null}, *Chm*^{Flox}, *Chm*^{WT} alleles (*top*) and control primers (*bottom*). (**C**) Eyes were collected from *Chm*^{WT}, *IRBP-Cre*+ animals at P21, stained with *Cre*-specific primary antibody and Alexa-568 secondary antibody, and visualized by confocal microscopy. (**D**) Phase image corresponding to (**C**). (**E**) In vitro prenylation reaction was performed on the cytosolic fractions of the lysates isolated from neuroretina (NR) and the RPE of the *Chm*^{WT}, *Chm*^{Flox}, and *Chm*^{Flox}, *IRBP-Cre*+ animals. (**F–I**) Paraffin wax sections were prepared from the eyes of *Chm*^{Flox} animals at 6 months (**F**) and 12 months (**H**) and *Chm*^{Flox}, *IRBP-Cre*+ animals at 6 months (**G**) and 12 months (**I**), cut at 4-μm thickness, and stained with hematoxylin and eosin.

supplemented with 0.5 μM RabGGTase, 0.5 μM REP1, 1 μM [^{3}H]-GGPP (Perkin Elmer, Wellesley, MA), 50 μM NP-40, 1 mM DTT, 50 mM HEPES, pH 7.2, and 5 mM $MgCl_2$ for 30 minutes at 37°C. The reaction mixture was separated on a 17.5% SDS-PAGE gel, which was then dried and exposed onto autoradiography film (Hyperfilm; GE Healthcare Biosciences, Piscataway, NJ). The protocol for immunoblotting has been described previously.[26]

Morphologic Studies

Mouse eyes for histology were fixed in 2% paraformaldehyde and 2.5% glutaraldehyde in 0.1 M cacodylate buffer for 1 hour. Samples were embedded in paraffin wax, and sections were cut at 4-μm thickness and stained with hematoxylin and eosin. Mouse eyes for immunohistochemistry were fixed in 4% paraformaldehyde in PBS for 1 hour, cryoprotected in 20% sucrose overnight, and embedded in the OCT compound. Sections were cut at 7-μm thickness and air-dried. *Cre*-specific antibody used for immunostaining was from Cambridge Bioscience (dilution 1:2500; Cambridge, UK). Iba-1–specific antibody was from MenaPath/A. Menarini Diagnostics Ltd. (dilution 1:1000; Berkshire, UK). For whole mount, eyes were fixed for 1 hour in 4% PFA in PBS, an incision was made along the ora serrata, five radial cuts were made to open the eyecup, and the neuroretina was gently peeled off. Electron microscopy was performed as described previously.[27]

Electroretinography and Scanning Laser Ophthalmoscopy

Before the ERG procedure, the mice were dark adapted (>1 hour), and the experimental preparation was performed under dim red illumination. The mice were anesthetized with a single intraperitoneal injection of medetomidine hydrochloride (Dormitor; 1 mg/kg body weight; Pfizer, New York, NY) and ketamine (60 mg/kg body weight) in water. The pupils were dilated using 1% tropicamide eyedrops. ERGs were recorded using an electroretinography console (Espion E^2; Diagnosys LLC, Cambridge, UK) that also generated and controlled the light stimulus. Single-flash stimuli were delivered in a Ganzfeld dome with the intensity increasing from −6 to 1 log cd · s/m^2 in 15 approximately half-log unit steps. For dim stimuli (−6 to −5 log cd · s/m^2), 10 responses were averaged with an interstimulus interval (ISI) of 2 seconds. For midrange stimuli (−4.523 to −2 log cd · s/m^2) 10 responses were averaged with an ISI of 5 seconds. For the brightest intensities (−1.523 to 1 log cd · s/m^2), five responses were averaged with an ISI of 10 seconds. A custom-made active electrode (platinum wire loop) was positioned concentrically to the cornea of the left eye using a micromanipulator. Hypromellose eyedrops (0.5% methylcellulose solution) were used to provide good electrical contact and to maintain corneal moisture. A reference electrode (subcutaneous stainless steel needle) was placed in the scruff, and an identical ground electrode was positioned at the base of the tail. Signals were differentially amplified and digitized at a rate of 5 kHz. Amplitudes of the major ERG components (a- and b-wave) were measured (Espion software; Diagnosys LLC) using automated and manual methods. Full datasets were tested for significant differences using two-way ANOVA, with genotype and light intensity as factors. Immediately after ERG recording, imaging of the fundus was performed with a scanning laser ophthalmoscope (HRA2; Heidelberg Engineering, Heidelberg, Germany), as previously described.[28]

Results

Photoreceptor-Specific *Chm KO*

To achieve a photoreceptor-specific *Chm* KO, we crossed *Chm^{Flox}* animals with an *IRBP-Cre* transgenic line, expressing *Cre*-recombinase under the control of the human *IRBP* promoter.[24] The *Chm^{Flox}* allele is a conditional allele that carries two *loxP* sites flanking exon 4, recombination between which leads to a frameshift and an early stop codon appearance[19] (Fig. 1A). To confirm the activity of the *IRBP-Cre* transgene,

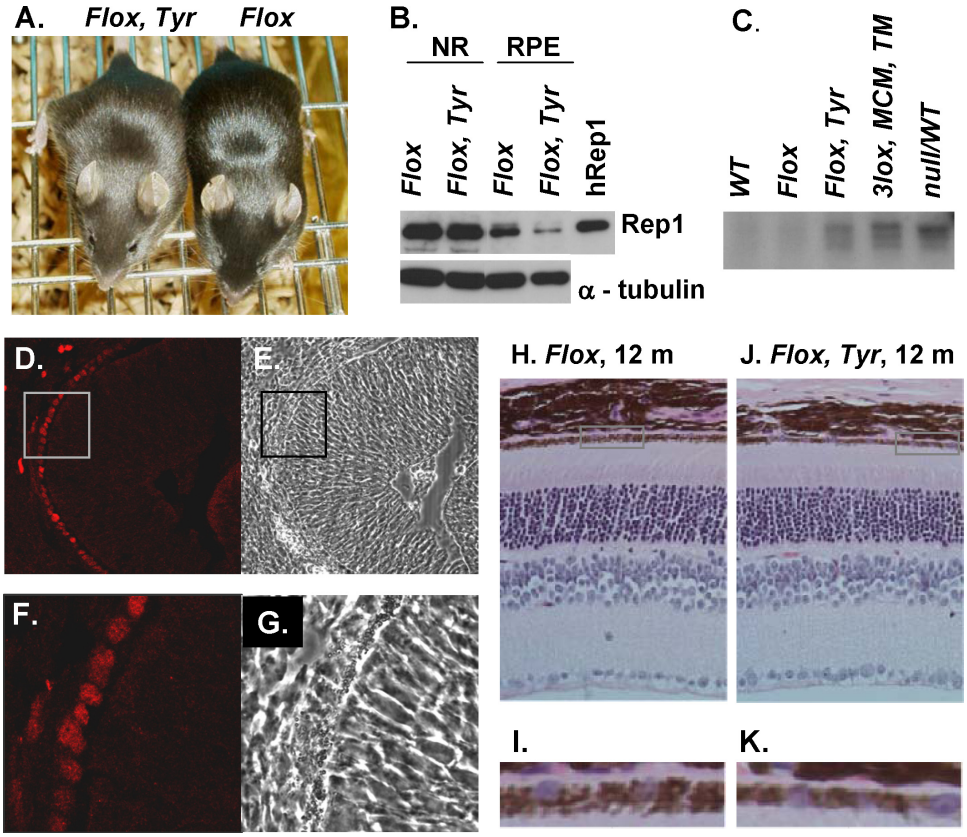

Figure 2. Characterization of *Chm^{Flox}*, *Tyr-Cre+* model (**A**) Photograph of 4-week-old *Chm^{Flox}*, *Tyr-Cre+* and *Chm^{Flox}* littermates. (**B**) Immunoblot analysis of the neuroretina (NR) and RPE cells isolated from the eyes of the *Chm^{Flox}* and *Chm^{Flox}*, *Tyr-Cre+* animals using Rep-specific antibody J905 and α-tubulin antibody (as a loading control). (**C**) In vitro prenylation reaction was performed on the cytosolic fractions of the lysates isolated from the RPE of the *Chm^{WT}*, *Chm^{Flox}*, *Chm$^{Null/WT}$*, TM-induced *Chm^{Flox}*, *MerCreMer+* and *Chm^{Flox}*, *Tyr-Cre+* animals. (**D–G**) Frozen section were prepared from *Chm^{WT}*, *Tyr-Cre+* animals at E12.5, stained with *Cre*-specific primary antibody and Alexa-568 secondary antibody, and visualized by confocal microscopy. (**E**) Phase image corresponding to (**D**). (**F**) Enlarged area of the *inset* in (**D**). (**G**) Phase image corresponding to (**F**). (**H–K**) Paraffin wax sections were prepared from the eyes of *Chm^{Flox}* (**H**) and *Chm^{Flox}*, *Tyr-Cre+* animal (**J**) at 1 year, cut at 4-μm thickness, and stained with hematoxylin and eosin. (**I**) Enlargement of the boxed area in (**H**). (**K**) Enlargement of the boxed area in (**J**).

the neuroretina and the RPE were isolated from the eyes of *Chm*^{Flox}, *IRBP-Cre*+ animals and were analyzed by PCR using pairs of primers that can identify *Chm*^{Flox}, *Chm*^{WT}, and *Chm*^{null} alleles simultaneously (Fig. 1B). The diagnostic 330-bp band was present in samples of the neuroretina from *Chm*^{Flox}, *IRBP-Cre*+ animals and in control *Chm*$^{null/WT}$ samples (RPE and neuroretina). To verify the expression of the *IRBP-Cre* transgene in the photoreceptors, we prepared frozen sections of the eyes of *Chm*^{WT}, *IRBP-Cre*+ mice at various time points: postnatal day (P) 14, P18, P21, and P70 and stained them with a *Cre*-specific antibody. We observed staining in the outer nuclear layer, consistent with expression of the transgene in the photoreceptors, that was maximal at P21, with >90% of photoreceptors expressing *Cre*-recombinase (Figs. 1C, 1D).

Next, we assessed the function of the Rep1 protein using an in vitro prenylation assay that identifies unprenylated Rabs that accumulate only when Rep1 is dysfunctional. Neuroretina and RPE were isolated from the eyes of *Chm*^{Flox}, *IRBP-Cre*+, and control (*Chm*^{Flox} and *Chm*^{WT}) animals. Cytosolic fractions were collected and subjected to an in vitro prenylation reaction using recombinant RabGGTase, REP1, and radiolabeled substrate [^{3}H]-geranylgeranyl pyrophosphate ([^{3}H]-GGPP), allowing visualization of the newly prenylated Rabs (Fig. 1E). As expected, there were no Rabs available for prenylation in the RPE of *Chm*^{Flox}, *IRBP-Cre*, and all control samples. Conversely, we observed radiolabeled bands after in vitro prenylation of Rabs (corresponding to unprenylated Rabs in vivo) in neuroretina samples obtained from *Chm*^{Flox}, *IRBP-Cre*+ eyes. This result confirms that photoreceptors exhibit a functional Rep1 defect.

Histologic analysis of the paraffin eye sections prepared from *Chm*^{Flox}, *IRBP-Cre*+ mice revealed slow progressive degeneration of photoreceptors (Figs. 1F-I), with a nearly normal thickness of the outer nuclear layer (ONL) in 6-month-old mice (8–10 rows of nuclei) and an approximately 30% reduction in 12-month-old mice (7–8 nuclei) compared with 10 to 12 nuclei for the control animals (*Chm*^{Flox}). Conversely, the RPE of *Chm*^{Flox}, *IRBP-Cre*+ animals demonstrated normal morphology with normal pigmentation and melanosome distribution in the apical processes (see Fig. 3C). Basal infoldings were regular and similar to those of the control samples (*Chm*^{Flox} and *Chm*^{WT}) (see Figs. 3A, 3B). Our data show that *Chm*^{Flox}, *IRBP-Cre*+ animals exhibited degeneration of photoreceptors in the presence of healthy RPE, confirming our previous finding that photoreceptors are a primary site of the disease.

RPE-Specific *Chm KO*

To achieve *Chm* KO specifically in the RPE, we used the transgenic line *Tyr-Cre* expressing *Cre*-recombinase under the control of an artificial tyrosinase promoter.[25] This promoter is active in pigmented cells, including RPE and skin melanocytes. *Chm*^{Flox}, *Tyr-Cre*+ animals have a lighter (chocolate) coat color than the *Chm*^{Flox} animals on the same C57BL/6 genetic background (Fig. 2A). This is presumably a result of the *Chm* deletion in melanocytes, which affects melanosome biogenesis and transport.[29] To determine whether the transgene was expressed in the RPE, we performed immunoblot analysis on isolated RPE and neuroretina from *Chm*^{Flox}, *Tyr-Cre*+ animals and showed that total amounts of Rep protein in the RPE of *Chm*^{Flox}, *Tyr-Cre*+ animals were markedly reduced compared with *Chm*^{Flox} animals (Fig. 2B). A small amount of Rep1 protein was still detectable, which could be derived from the outer segment discs shed from the overlying photoreceptors in which Rep1 was present. There was no difference between the expression level of Rep1 protein in *Chm*^{Flox}, *Tyr-Cre*+ and *Chm*^{Flox} animals in the respective neuroretina samples.

Next, we isolated cytosolic fractions from RPE cells of *Chm*^{Flox}, *Tyr-Cre*+ mice and performed in vitro prenylation (Fig. 2C). As positive controls, we used *Chm*$^{Null/WT}$ and TM-induced *Chm*^{3lox}, *MerCreMer*+ animals with significant RPE defects, as described in our previous study.[19] We observed bands corresponding to unprenylated Rabs in *Chm*^{Flox}, *Tyr-Cre*+ animals that were similar to *Chm*$^{Null/WT}$ and TM-induced *Chm*^{3lox}, *MerCreMer*+ animals,[19] confirming a prenylation defect in the RPE of the *Chm*^{Flox}, *Tyr-Cre*+ mice. To further demonstrate the *Chm* KO in the RPE, we observed positive staining in this layer after immunohistochemistry on frozen eye sections of the *Chm*^{WT}, *Tyr-Cre*+ embryos at embryonic day (E) 12.5 using *Cre*-specific antibody, confirming that the expression of the transgene in RPE occurred relatively early in eye development (Figs. 2D-G).

Retinal morphology of *Chm*^{Flox}, *Tyr-Cre*+ animals was analyzed at 6, 12, and 19 months. There was no obvious pathology, including no apparent reduction in the number of photoreceptors as determined by counting the rows of nuclei in the ONL (Figs. 2H-K). Electron microscopy was used to analyze the morphology of the RPE in more detail (Fig. 3). In the samples from *Chm*^{Flox}, *Tyr-Cre*+ animals we observed pigment irregularities (Fig. 3F). More specifically, melanosome distribution was not homogeneous throughout the RPE, and in some areas melanosomes remained in the main body of the cell and did not enter apical processes as seen in wild-type mice. This is a

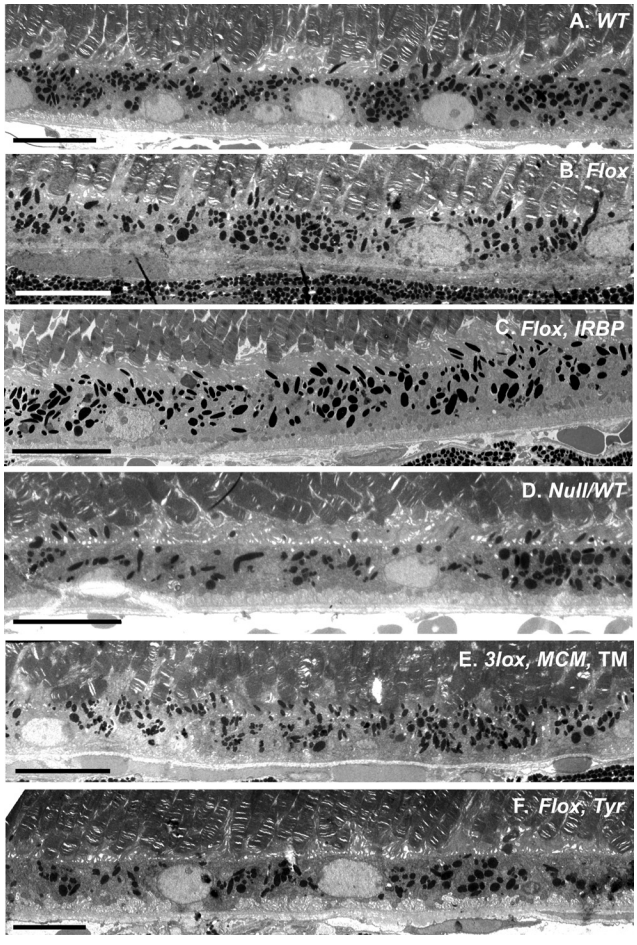

FIGURE 3. Electron microscopy of the *Chm*^{WT} (**A**), *Chm*^{Flox} (**B**), *Chm*^{Flox}, *IRBP-Cre*+ (**C**), *Chm* $^{Null/WT}$ (**D**), TM -induced *Chm*^{3lox}, *MerCreMer*+ (**E**), *Chm*^{Flox}, *Tyr-Cre*+ (**F**) at 5 months. In (**A**), (**B**), (**C**), and (**E**), the RPE is highly pigmented, and melanosomes are found in apical processes. In contrast, in (**F**) and some areas of (**D**), pigmentation is altered and melanosomes remain in the cell body. Scale bar, 10 μm.

hallmark of Rab27a dysfunction, also observed in Rab27a mutant (*ashen*) mice.[30] Another striking feature was disorganization of basal infoldings. In contrast to control mice (Figs. 3A, 3B), basal infoldings in all RPE-KO mice lost their regular thickness and organization ($Chm^{null/WT}$, Fig. 3D; TM-induced Chm^{3lox}, *MerCreMer*+, Fig. 3E; Chm^{Flox}, *Tyr-Cre*+, Fig. 3F).[19] Overall, the data confirm our previous conclusion that the RPE and photoreceptors degenerate because of intrinsic defects in each layer that do not lead to a significant secondary degeneration of the other layer.[19] Hence, both layers could be considered the primary pathogenic sites in CHM.

Double-Layer *Chm KO*

To test whether one layer could influence the adjacent layer, we produced mice with the *Chm* KO in both photoreceptors and RPE cells (Chm^{Flox}, *IRBP-Cre*+, *Tyr-Cre*+). Histopathologic studies were performed in paraffin wax-embedded eyes (Fig. 4). In 6- to 8-month-old Chm^{Flox}, *IRBP-Cre*+, *Tyr-Cre*+ mice, we observed a sharp decline in the number of photoreceptors (Fig. 4D) compared with control and single-layer KO strains (Figs. 4A-C). Nevertheless, the degeneration remained stable and, by 12 to 14 months, the photoreceptor KO and the double KO exhibited similar levels of photoreceptor degeneration (compare Figs. 1I and 4F). Results of a quantitative assessment are presented in Figure 4G. Our data suggest that the degeneration of *Chm* photoreceptors was accelerated in the presence of *Chm* RPE in younger mice but later became level and approached that seen in the presence of wild-type RPE.

Electrophysiological Analysis of *Chm KO* Mice

Next, we assessed the retinal function of the newly generated *Chm* mouse strains. First, we recorded electroretinograms (ERGs) for all the genotypes of two different ages (8 and 14 months). We recorded single-flash scotopic intensity series and, in all animals tested, observed the major components of the ERG (a-wave, b-wave, oscillatory potentials). The amplitude of a- and b-waves was quantified and compared between the genotypes (Fig. 5). In all cases, the presence and magnitude of these components was intensity dependent. At 8 months, there were significant differences in the a-wave amplitude among all three models ($P < 0.0072$, genotype as factor in two-way ANOVA). The a-wave is an early negative deflection of the ERG and reflects activation of the photoreceptors (primarily the rods). Chm^{Flox}, *IRBP-Cre*+, *Tyr-Cre*+ animals showed reduced a-wave amplitudes across all intensities, consistent with a degenerate or dysfunctional photoreceptor layer. Chm^{Flox}, *Tyr-Cre*+ animals exhibited reduced amplitude a-waves, suggesting that *Chm* KO in the RPE can affect the photoreceptor function/physiology without causing any obvious photoreceptor degeneration. Responses of Chm^{Flox}, *IRBP-Cre*+ mice were indistinguishable from those of control Chm^{Flox} animals, which was in accordance with the good preservation of the retina and only minor changes in histology observed at this age.

There were no significant differences in b-wave amplitude among the groups at 8 months. The b-wave immediately follows the a-wave, and the positive potential is thought to reflect the activity of inner retinal neurons, particularly ON bipolar cells. Because the b-wave derives from second-order neurons, it is necessarily dependent on the magnitude of photoreceptor activation and also on the status of synaptic transmission. In addition, as the amplitude of the b-wave is measured from the base of the a-wave, it inherently incorporates both responses and is a good measure of the overall electrical activation. There seemed to be a reduction in b-wave amplitude in Chm^{Flox}, *IRBP-Cre*+, *Tyr-Cre*+ animals, especially at higher intensities. This probably resulted from the reduced a-wave amplitude seen in the same group, but the difference was not large enough to be significant ($P < 0.0534$, genotype as factor in two-way ANOVA).

Analysis of older mice (13–14 months) revealed highly significant differences in a- and b-wave amplitude between the transgenic models (genotype was a significant factor in two-

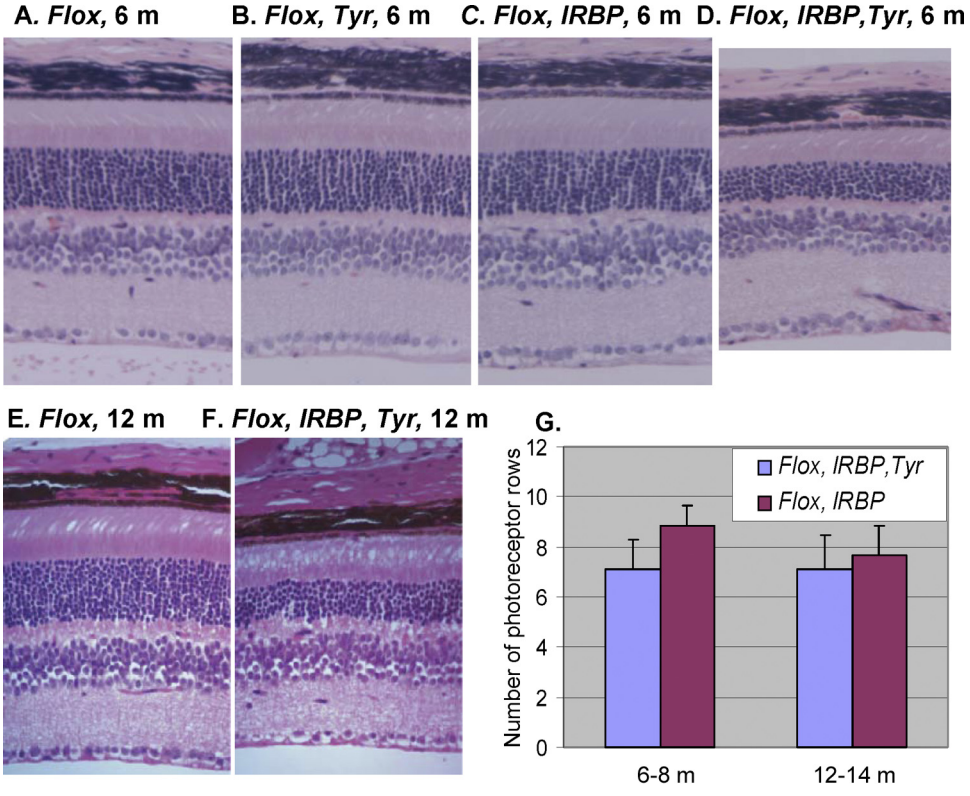

FIGURE 4. Histologic analysis of the retina of the 6-month old Chm^{Flox} (**A**), Chm^{Flox}, *Tyr-Cre*+ (**B**), Chm^{Flox}, *IRBP-Cre*+ (**C**) , Chm^{Flox}, *IRBP-Cre*+, *Tyr-Cre*+ (**D**) and 12-month old Chm^{Flox} (**E**), *IRBP-Cre*+, *Tyr-Cre*+ (**F**). (**G**) Morphometric analysis of the number of photoreceptor rows in the central retina in the Chm^{Flox}, *IRBP-Cre*+ (purple bars) and Chm^{Flox}, *IRBP-Cre*+, *Tyr-Cre*+ (*blue bars*). Numbers of animals analyzed were: Chm^{Flox}, *IRBP-Cre*+: 6 to 8 months ($n = 15$), 12 to 14 months ($n = 19$); Chm^{Flox}, *IRBP-Cre*+, *Tyr-Cre*+: 6 to 8 months ($n = 7$), 12 to 14 months ($n = 11$).

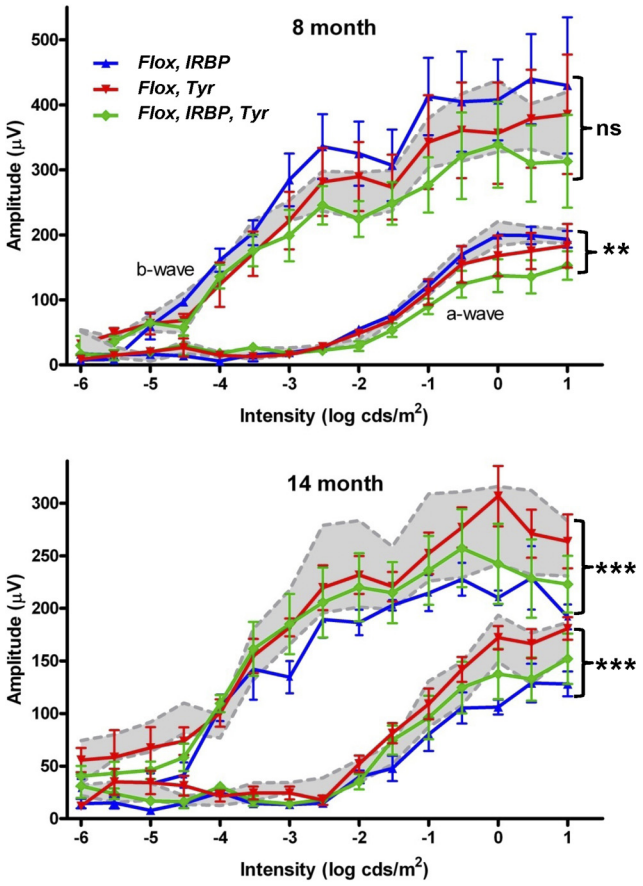

FIGURE 5. Quantification of the amplitude of the major components (a- and b-wave) of the dark-adapted ERG across a range of stimulus intensity. Two groups of animals (8-month- and 14-month-old) were studied. Numbers of 8-month-old animals were: *Chm*^{Flox}, *Tyr-Cre*+ (n = 5); *Chm*^{Flox}, *IRBP-Cre*+ (n = 3); *Chm*^{Flox}, *Tyr-Cre*+, *IRBP-Cre*+ (n = 5), and *Chm*^{Flox} (n = 4). Numbers of 14-month-old animals were: *Chm*^{Flox}, *Tyr-Cre*+ (n = 6); *Chm*^{Flox}, *IRBP-Cre*+ (n = 5); *Chm*^{Flox}, *Tyr-Cre*+, *IRBP-Cre*+ (n = 6), and *Chm*^{Flox} (n = 6). All genotypes are shown on each graph: *Chm*^{Flox}, *Tyr-Cre*+ (*red line*), *Chm*^{Flox}, *IRBP-Cre*+ (*blue line*), *Chm*^{Flox}, *IRBP-Cre*+, *Tyr-Cre*+ (*green line*). Mean amplitudes ± SEM are plotted. Values for control animals (*Chm*^{Flox}, mean ± SEM) are indicated by *gray shading*.

way ANOVA; $P < 0.0001$ in both cases). In general the amplitude of ERGs in the older cohort was lower than those in younger mice (although there were exceptions for a-wave amplitude). A normal age-related decline in the ERG amplitude of wild-type C57BL/6 mice has been described.[28] Importantly, older *Chm*^{Flox}, *IRBP-Cre*+ animals, which showed no deficit at 8 months, showed a strong age-related decline and now demonstrated the lowest amplitude responses of all groups for both a- and b-waves. The ERGs of older *Chm*^{Flox}, *Tyr-Cre*+ mice were identical with *Chm*^{Flox} controls. The mild a-wave deficit seen in younger *Chm*^{Flox}, *Tyr-Cre*+ animals was no longer present, suggesting that this strain did not exhibit any age-related decline. The *Chm*^{Flox}, *Tyr-Cre*+ group continued to show lower amplitude responses compared with control, though the magnitude of this difference was perhaps reduced with age. Again, with a-wave amplitude, this convergence seemed to arise from an absence or a reduction in the age-related decline in the *Chm*^{Flox}, *Tyr-Cre*+ compared with the control group. Taken together, these data demonstrate that anatomic changes in the RPE and neuroretina are reflected in changes in function. The data also point to some interesting interactions between aging and layer-specific *Chm* KO.

Scanning Laser Ophthalmoscopy Analysis of *Chm KO mice*

In the same cohort of animals, a scanning laser ophthalmoscope (SLO) was used with autofluorescent (AF) visualization to investigate the pathologic changes of the fundus in vivo (Fig. 6). For *Chm*^{Flox}, *Tyr-Cre*+ mice, we observed abnormal autofluorescent mottling of the retina that was equally obvious at 8 and 14 months (Figs. 6B, 6F, 6J) and was consistent with pigment irregularities found in these animals by electron microscopy (Fig. 3E). *Chm*^{Flox}, *IRBP-Cre*+ mice exhibited a dramatic change from the ostensibly normal appearance of the fundus in the 8-month-old animals (Fig. 6C) to the multiple dot-shape autofluorescent spots of the retina in the older animals (14 months) (Figs. 6G, 6K). Abnormal autofluorescence of both types (mottling and dot-like specks) was present in 8- and 14-month-old *Chm*^{Flox}, *IRBP-Cre*+, *Tyr-Cre*+ mice in abundance.

To establish the origin of these autofluorescent dot-like structures, we prepared whole mounts and stained them with antibody specific for ionized calcium adapter molecule (Iba-1), a marker for cells of microglia origin (Fig. 7). We observed punctate staining that resembled the SLO images, suggesting that at least some of the autofluorescent dots are of microglia origin (Figs. 7A, 7B). Quantification of the Iba-1–positive structures showed a significant increase in the number of these cells in *Chm*^{Flox}, *IRBP-Cre*+, *Tyr-Cre*+ animals compared with *Chm*^{Flox}, *IRBP-Cre*+ and *Chm*^{Flox}, *Tyr-Cre*+ strains (Fig. 7C). Overall these data further suggest that the dynamics of retinal degeneration are altered when both photoreceptors and RPE contain the *Chm* mutation.

DISCUSSION

The aim of this study was to dissect the complex pathologic changes involving photoreceptors and RPE that occur during the CHM retinal degenerative process. For this, we created two new cell layer–specific *Chm* KO models: *Chm*^{Flox}, *IRBP-Cre*+ (photoreceptor-specific) and *Chm*^{Flox}, *Tyr-Cre*+ (RPE-specific) and produced a double transgenic line (*Chm*^{Flox}, *IRBP-Cre*+, *Tyr-Cre*+). The main novel finding we report here is that the combination of RPE and photoreceptor disease is not equivalent to the sum of the effects observed in each cell type. We observed enhanced functional defects and photoreceptor cell loss in younger double transgenic mice, implying that the presence of a diseased RPE impacts the rate of photoreceptor degeneration. Therefore, this study highlighted that the adjacent cell layers in the eye influence each other and that these interactions are important factors that determine the CHM retinal degenerative process. Despite these significant novel findings, the results of this study are consistent with our previous results because they further support the idea that both layers are primary sites of CHM disease.[19] We observed slow, progressive degeneration of photoreceptors but normal RPE in the photoreceptor-specific KO and RPE abnormalities but normal photoreceptors in the RPE-specific line.

The combined histologic and functional data reported here suggest a complex relationship between the survival and function of photoreceptors, RPE status, and aging. First, there was a mild but consistent decrease in a-wave amplitude in younger (8-month) *Chm*^{Flox}, *Tyr-Cre*+ animals in comparison with *Chm*^{Flox} control mice. *Chm*^{Flox}, *Tyr-Cre*+ animals retain a normal ONL thickness into advanced age (>1.5 years) and it seems likely, therefore, that the a-wave deficit was caused by an indirect impairment of photoreceptors because of changes in the function of the choroiderremic RPE. Importantly, the a-wave deficit receded in older

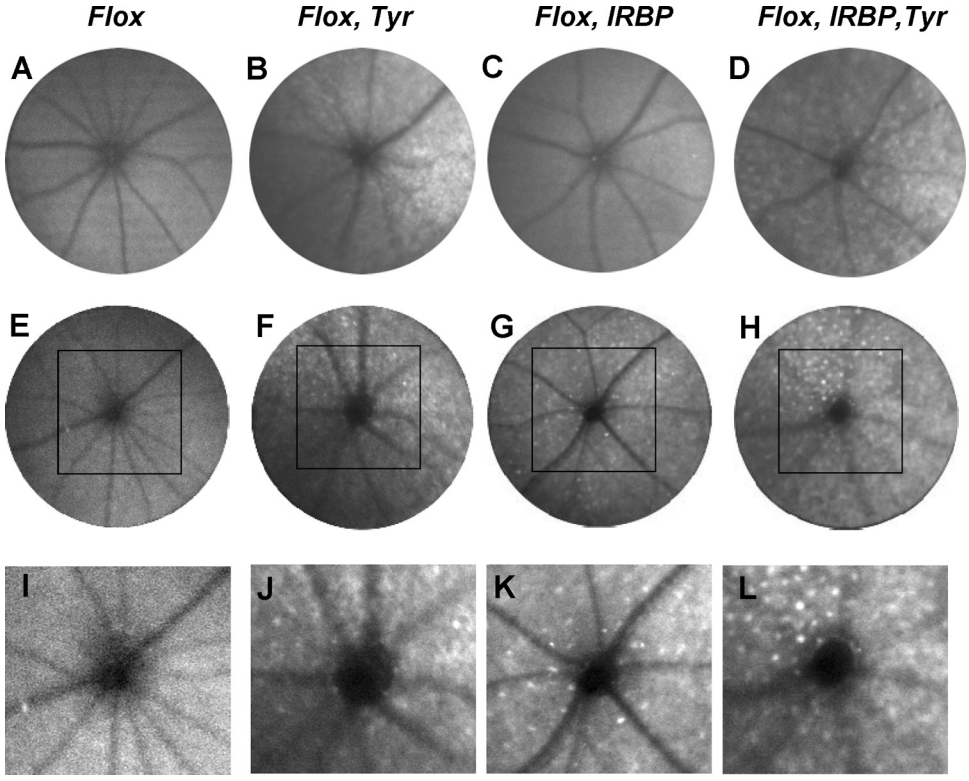

FIGURE 6. Representative AF-SLO projection fundus images obtained from *Chm*^{Flox} (**A**, **E**, **I**), *Chm*^{Flox}, *Tyr-Cre+* (**B**, **F**, **J**), *Chm*^{Flox}, *IRBP-Cre+* (**C**, **G**, **K**), *Chm*^{Flox}, *IRBP-Cre+*, *Tyr-Cre+* (**D**, **H**, **L**) at 8 months (**A–D**) and 14 months (**E–L**). (**I–L**) Enlargement of the *boxed area* in (**E–H**).

Chm^{Flox}, *Tyr-Cre+* animals, suggesting that *Chm* KO in the RPE somehow functionally mimics the normal aging processes. This possibility is exciting and certainly warrants further investigation. Second, we found a considerable increase in the rate of photoreceptor degeneration in combined photoreceptor and RPE *Chm* KO (*Chm*^{Flox}, *IRBP-Cre+*, *Tyr-Cre+*) in comparison with photoreceptor *Chm* KO (*Chm*^{Flox}, *IRBP-Cre+*). Therefore, choroideremic changes in photoreceptors and RPE do not progress independently. Interestingly however, the photoreceptor *Chm* KO alone eventually exhibited levels of photoreceptor degeneration similar to those of the double *Chm* KO, suggesting that the diseased RPE does not have an additive detrimental effect on ultimate *Chm* KO photoreceptor survival. These observations further suggest that the *Chm* RPE may behave as a prematurely aged RPE. Third, we observed a significantly increased amount of microglia cells in the double *Chm* KO, which are scavenging cells presumably recruited to clear the debris produced by dying photoreceptors, in agreement with the increased rate of photoreceptor degeneration in these mice. Similar observations were reported in other recently published studies.[28,31,32] Interestingly, retinal thickening was observed in early-stage CHM patients and was proposed to be a surrogate marker for retinal remodeling through Müller (microglia) cell hypertrophy.[33] This study is consistent with that hypothesis. Fourth, we report the surprising observation that the double *Chm* KO had less ERG suppression at 14 months than the photoreceptor *Chm* KO. This might have been an artifact caused by a nonretinal factor relevant to these mice because it is known that tyrosinase is expressed in some neuronal cells, where it is proposed to contribute to the formation of neuromelanin.[34] Alternatively, it could be that the absence of Rep1 in the RPE somehow partially compensates for the reduced amplitude normally present in the photoreceptor-specific KO, possibly by electrical changes such as improved conductance occurring as a result of impaired vesicle transport.

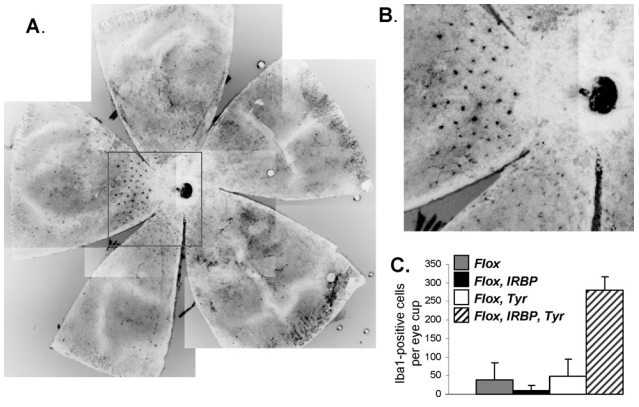

FIGURE 7. (**A**) Retinal flat mounts from an 11-month-old *Chm*^{Flox} *IRBP-Cre+*, *Tyr-Cre+* animal were stained with anti–Iba1 primary and anti–rabbit Alexa-488 secondary antibody. (**B**) Enlargement of the *boxed area* in (**A**). (**C**) Quantitative data of the number of Iba1-positive cells per eye cup from 11- to 12-month-old *Chm*^{Flox} (*gray bar*), *Chm*^{Flox}, *IRBP-Cre+* (*closed bar*), *Chm*^{Flox}, *Tyr-Cre+* (*open bar*), and *Chm*^{Flox}, *IRBP-Cre+*, *Tyr-Cre+* (*hatched bar*) animals.

We observed mild functional impairment of photoreceptors that were morphologically normal in the RPE *Chm* KO. Hence, our model supports the notion that CHM is a retinal disease that initially causes sight impairment by functional defects and that cell death occurs later. This would be highly relevant for potential gene therapy because any functional deficit might be reversed by expression of the transgenic REP1 in photoreceptor cells. Because both layers could be considered primary sites of the disease, it is logical to propose that future gene therapy approaches for CHM should use viral vectors that target both photoreceptors and RPE. This would include adeno-associated virus (AAV) serotype 2, which has been shown to be safe and effective after subretinal delivery in several patients in preliminary reports from

three ongoing clinical trials.[35–37] Future studies should address the hypotheses suggested by the present study. Additionally, it will be important to study the involvement of the choroid, particularly the choriocapillaris,[38] in the pathogenesis of CHM.

Acknowledgments

The authors thank Anton Berns and Lionel Larue for transgenic mouse strains, Richard Marais and Robert Hayward for the help with obtaining the animals, Glen Jeffery, Marcus Fruttiger, and Jaimie Hoh Kam for valuable discussions on microglia cells and help with the whole mount preparation, Dhani Tracey-White for assistance with animal care and genotyping, and Abul Tarafder for stimulating discussions.

References

1. Cremers FPM, Ropers H. Choroideremia. In: Scriver CR, Beaudet AL, Sly WS, et al., eds. *The Metabolic and Molecular Bases of Inherited Disease*. New York: McGraw-Hill, Inc.; 2001:5935–5945.
2. Heckenlively JR, Bird AJ. Choroideremia. In: Heckenlively JR, ed. *Retinitis Pigmentosa*. Philadelphia: JB Lippincott; 1988:176–187.
3. McCulloch C. Choroideremia and other choroidal atrophies. In: Newsome DA, ed. *Retinal Dystrophies and Degenerations*. New York: Raven Press; 1988:285–295.
4. MacDonald IM, Sereda C, McTaggart K, Mah D. Choroideremia gene testing. *Expert Rev Mol Diagn.* 2004;4:478–484.
5. Yau RJ, Sereda CA, McTaggart KE, Sauve Y, MacDonald IM. Choroideremia carriers maintain a normal electro-oculogram (EOG). *Doc Ophthalmol.* 2007;114:147–151.
6. Bonilha VL, Trzupek KM, Li Y, et al. Choroideremia: analysis of the retina from a female symptomatic carrier. *Ophthalmic Genet.* 2008;29:99–110.
7. Renner AB, Kellner U, Cropp E, et al. Choroideremia: variability of clinical and electrophysiological characteristics and first report of a negative electroretinogram. *Ophthalmology.* 2006;113:2066–2073.
8. Cremers FP, van de Pol DJ, van Kerkhoff LP, Wieringa B, Ropers HH. Cloning of a gene that is rearranged in patients with choroideraemia. *Nature.* 1990;347:674–677.
9. Seabra MC, Brown MS, Slaughter CA, Sudhof TC, Goldstein JL. Purification of component A of Rab geranylgeranyl transferase: possible identity with the choroideremia gene product. *Cell.* 1992; 70:1049–1057.
10. Pylypenko O, Rak A, Reents R, et al. Structure of Rab escort protein-1 in complex with Rab geranylgeranyltransferase. *Mol Cell.* 2003;11:483–494.
11. Merithew E, Hatherly S, Dumas JJ, Lawe DC, Heller-Harrison R, Lambright DG. Structural plasticity of an invariant hydrophobic triad in the switch regions of Rab GTPases is a determinant of effector recognition. *J Biol Chem.* 2001;276:13982–13988.
12. Fukuda M. Versatile role of Rab27 in membrane trafficking: focus on the Rab27 effector families. *J Biochem (Tokyo).* 2005; 137:9–16.
13. Pereira-Leal JB, Seabra MC. The mammalian Rab family of small GTPases: definition of family and subfamily sequence motifs suggests a mechanism for functional specificity in the Ras superfamily. *J Mol Biol.* 2000;301:1077–1087.
14. Stenmark H. Rab GTPases as coordinators of vesicle traffic. *Nat Rev Mol Cell Biol.* 2009;10:513–525.
15. Jordens I, Marsman M, Kuijl C, Neefjes J. Rab proteins, connecting transport and vesicle fusion. *Traffic.* 2005;6:1070–1077.
16. Cremers FP, Armstrong SA, Seabra MC, Brown MS, Goldstein JL. REP-2, a Rab escort protein encoded by the choroideremialike gene. *J Biol Chem.* 1994;269:2111–2117.
17. Shi W, van den Hurk JA, Alamo-Bethencourt V, et al. Choroideremia gene product affects trophoblast development and vascularization in mouse extra-embryonic tissues. *Dev Biol.* 2004; 272:53–65.
18. van den Hurk JA, Hendriks W, van de Pol DJ, et al. Mouse choroideremia gene mutation causes photoreceptor cell degeneration and is not transmitted through the female germline. *Hum Mol Genet.* 1997;6:851–858.
19. Tolmachova T, Anders R, Abrink M, et al. Independent degeneration of photoreceptors and retinal pigment epithelium in conditional knockout mouse models of choroideremia. *J Clin Invest.* 2006;116:386–394.
20. Starr CJ, Kappler JA, Chan DK, Kollmar R, Hudspeth AJ. Mutation of the zebrafish choroideremia gene encoding Rab escort protein 1 devastates hair cells. *Proc Natl Acad Sci U S A.* 2004;101:2572–2577.
21. Moosajee M, Tulloch M, Baron RA, Gregory-Evans CY, Pereira-Leal JB, Seabra MC. Single choroideremia gene in nonmammalian vertebrates explains early embryonic lethality of the zebrafish model of choroideremia. *Invest Ophthalmol Vis Sci.* 2009;50:3009–3016.
22. Krock BL, Bilotta J, Perkins BD. Noncell-autonomous photoreceptor degeneration in a zebrafish model of choroideremia. *Proc Natl Acad Sci U S A.* 2007;104:4600–4605.
23. Syed N, Smith JE, John SK, Seabra MC, Aguirre GD, Milam AH. Evaluation of retinal photoreceptors and pigment epithelium in a female carrier of choroideremia. *Ophthalmology.* 2001;108:711–720.
24. Vooijs M, te Riele H, van der Valk M, Berns A. Tumor formation in mice with somatic inactivation of the retinoblastoma gene in interphotoreceptor retinol binding protein-expressing cells. *Oncogene.* 2002;21:4635–4645.
25. Delmas V, Martinozzi S, Bourgeois Y, Holzenberger M, Larue L. Cre-mediated recombination in the skin melanocyte lineage. *Genesis.* 2003;36:73–80.
26. Tolmachova T, Anders R, Stinchcombe J, et al. A general role for Rab27a in secretory cells. *Mol Biol Cell.* 2004;15:332–344.
27. Futter CE, Ramalho JS, Jaissle GB, Seeliger MW, Seabra MC. The role of Rab27a in the regulation of melanosome distribution within retinal pigment epithelial cells. *Mol Biol Cell.* 2004;15:2264–2275.
28. Luhmann UF, Robbie S, Munro PM, et al. The drusenlike phenotype in aging Ccl2 knockout mice is caused by an accelerated accumulation of swollen autofluorescent subretinal macrophages. *Invest Ophthalmol Vis Sci.* 2009;50:5934–5943.
29. Wasmeier C, Hume AN, Bolasco G, Seabra MC. Melanosomes at a glance. *J Cell Sci.* 2008;121:3995–3999.
30. Lopes VS, Ramalho JS, Owen DM, et al. The ternary Rab27a-Myrip-Myosin VIIa complex regulates melanosome motility in the retinal pigment epithelium. *Traffic.* 2007;8:486–499.
31. Xu H, Chen M, Manivannan A, Lois N, Forrester JV. Age-dependent accumulation of lipofuscin in perivascular and subretinal microglia in experimental mice. *Aging Cell.* 2008;7:58–68.
32. Mendes-Jorge L, Ramos D, Luppo M, et al. Resident autofluorescent perivascular macrophages have a scavenger function and may contribute to the maintenance of the blood-retinal barrier. *Invest Ophthalmol Vis Sci.* 2009;50:5997–6005.
33. Jacobson SG, Cideciyan AV, Sumaroka A, et al. Remodeling of the human retina in choroideremia: rab escort protein 1 (REP-1) mutations. *Invest Ophthalmol Vis Sci.* 2006;47:4113–4120.
34. Greggio E, Bergantino E, Carter D, et al. Tyrosinase exacerbates dopamine toxicity but is not genetically associated with Parkinson's disease. *J Neurochem.* 2005;93:246–256.
35. Bainbridge JW, Smith AJ, Barker SS, et al. Effect of gene therapy on visual function in Leber's congenital amaurosis. *N Engl J Med.* 2008;358:2231–2239.
36. Maguire AM, Simonelli F, Pierce EA, et al. Safety and efficacy of gene transfer for Leber's congenital amaurosis. *N Engl J Med.* 2008;358:2240–2248.
37. Kaplitt MG, Feigin A, Tang C, et al. Safety and tolerability of gene therapy with an adeno-associated virus (AAV) borne GAD gene for Parkinson's disease: an open label, phase I trial. *Lancet.* 2007;369:2097–2105.
38. Cameron JD, Fine BS, Shapiro I. Histopathologic observations in choroideremia with emphasis on vascular changes of the uveal tract. *Ophthalmology.* 1987;94:187–196.